Electron and hole contributions to normal-state transport in the superconducting system $Sn_{1-x}In_xTe$

Cheng Zhang,[1,2,*] Xu-Gang He,[1,3] Hang Chi,[1] Ruidan Zhong,[1,2,†] Wei Ku,[1,‡] Genda Gu,[1] J. M. Tranquada,[1] and Qiang Li[1,§]

[1]*Condensed Matter Physics and Materials Science Division, Brookhaven National Laboratory, Upton, New York 11973, USA*
[2]*Materials Science and Engineering Department, Stony Brook University, Stony Brook, New York 11794, USA*
[3]*Department of Physics and Astronomy, Stony Brook University, Stony Brook, New York 11794, USA*

Indium-doped SnTe has been of interest because the system can exhibit both topological surface states and bulk superconductivity. While the enhancement of the superconducting transition temperature is established, the character of the electronic states induced by indium doping remains poorly understood. We report a study of magnetotransport in a series of $Sn_{1-x}In_xTe$ single crystals with $0.1 \leqslant x \leqslant 0.45$. From measurements of the Hall effect, we find that the dominant carrier type changes from holelike to electronlike at $x \sim 0.25$; one would expect electronlike carriers if the In ions have a valence of $+3$. For single crystals with $x = 0.45$, corresponding to the highest superconducting transition temperature, pronounced Shubnikov–de Haas oscillations are observed in the normal state. In measurements of magnetoresistance, we find evidence for weak antilocalization (WAL). We attribute both the quantum oscillations and the WAL to bulk Dirac-like hole pockets, previously observed in photoemission studies, which coexist with the dominant electronlike carriers.

I. INTRODUCTION

The discovery of topological insulators (TIs) has attracted great attention and stimulated considerable work on topological surface states arising from band inversion and time-reversal symmetry [1–3]. In topological states, electrons can flow with much reduced scattering from nonmagnetic defects, offering great promise for next-generation electronics. Crystalline symmetry was soon identified as another promising route for obtaining the protected metallic surface states, leading to the new category of topological crystalline insulators (TCIs) [4]. Tin telluride is a prototypical TCI predicted to have four conducting surface channels on specific crystallographic planes [5,6]. The band inversion has been confirmed, and surface states have been observed, by angle-resolved photoemission spectroscopy (ARPES) [7,8]. Experimental evidence for topologically nontrivial surface states has been obtained in transport studies of thin films [9,10]. It has been proposed theoretically that combining topological surface states with bulk superconductivity may yield Majorana modes, which are of interest for use in quantum computing schemes [11,12]. Given that superconductivity can be induced in the SnTe system by indium doping, where the transition temperature can be as high as 4.5 K [13–15], it is a natural system in which to look for the desired combination of states [16].

An unresolved issue concerns the nature of the carriers introduced by In doping. Studies of IV-VI semiconductors have long indicated that In dopants act as if they contribute a resonance state or impurity band near the Fermi level [17]. A relevant comparison is to Tl-doped PbTe, where the Tl^{+1} and Tl^{+3} states may be nearly degenerate [18,19]. Hall effect measurements on $Sn_{1-x}In_xTe$ (SIT) with $x \lesssim 0.1$ indicate than In induces an enhanced density of holes [13,20]. Angle-resolved photoemission spectroscopy (ARPES) studies of SIT have demonstrated the presence of small, holelike Fermi pockets at the L points of the Brillouin zone from both bulk and surface states for x as large as 0.4 [7,8,21,22]. In contrast, recent measurements of the Hall effect on polycrystalline samples indicate a change in carrier type from holes to electrons on increasing x beyond 10% [23]. Indeed, supercell calculations of the band structure for SIT at small x indicate the presence of an In-induced electronlike band crossing the Fermi level [23].

In this paper we use transport measurements to explore the normal-state properties of $Sn_{1-x}In_xTe$ single crystals for $0.1 \leqslant x \leqslant 0.45$, spanning most of the range of superconductivity. From measurements of the Hall coefficient at $T = 5$ K, we infer the presence of both hole- and electronlike charge carriers, with a crossover in the dominant type at $x \sim 0.25$. The significant change with increasing x is the increase in electron mobility. In field-dependent measurements of the Hall coefficient, we observe Shubnikov–de Haas oscillations, whose frequency and temperature-dependent amplitude are comparable to those expected for the bulk L-point hole pockets as detected by ARPES [21,22]. We also observe positive magnetoresistance that bears the signature of weak antilocalization (WAL). As the magnitude of the magnetoresistance is independent of the orientation of the magnetic field, we attribute it to the bulk hole pockets and their Dirac-like character [22,24]. Overall, we find that the transport properties can be modeled in a consistent fashion by taking account of both the holelike and electronlike carriers.

―――――――

*Present address: Department of Materials Science and Engineering, University of Tennessee, Knoxville, Tennessee, USA.

†Present address: Department of Chemistry, Princeton University, Princeton, New Jersey 08544, USA.

‡Present address: School of Physics and Astronomy, Shanghai Jiao Tong University, Shanghai 200240, China.

§qiangli@bnl.gov
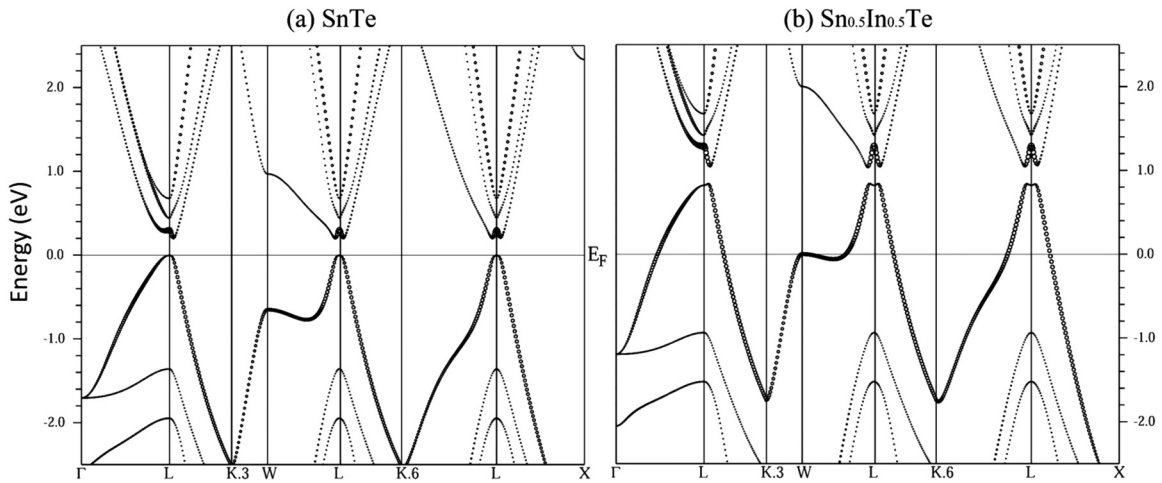
(a) SnTe   (b) $Sn_{0.5}In_{0.5}Te$

FIG. 1. First-principles band structure of (a) SnTe and (b) $Sn_{0.5}In_{0.5}Te$. Applying the VCA method to the occupancy of the Sn $5s$ orbital, the impact of the In substitution is to push the Fermi level down into the valence band, reaching a level of 0.8 eV below the top of the valence band. The overall band structure remains intact, but with an enhancement of the band inversion.

II. EXPERIMENTAL METHODS

Single crystals of $Sn_{1-x}In_xTe$ (SIT) with nominal In concentrations of $x = 0.10$–0.45 were grown by a modified floating-zone method. Pure SnTe used in the experiment was a polycrystalline sample, prepared via the horizontal unidirectional solidification method. The details were reported previously [15]. Crystals were cut into thin (~0.4 mm) strips along (100) planes (with an orientational uncertainty of $5°$), and measured in a Quantum Design Physical Property Measurement System (PPMS) equipped with a 9 T magnet. A photo of a typical sample prepared for transport measurement is shown in the inset of Fig. 2(a). The longitudinal resistivity was measured using a standard four probe method with in-line configuration. Hall measurement was conducted with voltage contacts placed on opposite sides of single crystals.

III. BAND-STRUCTURE CALCULATIONS

To provide context for interpreting the measurements, we did some simple band-structure calculations. We consider the case in which each indium dopant replaces a Sn atom and behaves as an acceptor, having one less electron than Sn. We used the WIEN2k code [25] to calculate the expected band structure using the virtual crystal approximation (VCA) to model the partial substitution of Sn by In. The results are shown in Fig. 1. The main change due to 50% In substitution is that the Fermi level moves deep into the valence band (0.8 eV from the top of the valence band), although the band inversion is also significantly enhanced compared to pure SnTe. ARPES measurements on a film with $x = 0.41$ demonstrate that the Fermi level is indeed in the hole band [22], although the shift from $x = 0$ [8] appears to be considerably smaller than the calculated value.

IV. TRANSPORT MEASUREMENTS

A. Doping dependence

The transport data for our SIT crystals spanning a range of In concentrations are presented in Fig. 2. In particular,

longitudinal electrical resistivity is shown as a function of temperature in Fig. 2(b), where the superconducting transition temperature clearly increases while the magnitude of the resistivity decreases with In doping. Figure 2(c) shows the temperature dependence of the carrier concentration N_H calculated from the Hall coefficient R_H using a single band model: $N_H = 1/(eR_H)$ (positive values for holes and negative for electrons), where e is the electron charge. A dramatic change in the carrier type from p type to n type is found between $x = 0.2$ and 0.3. The sign change is qualitatively consistent with the results of Haldolaarachchige *et al.* [23] measured on polycrystalline samples. (We do not have a clear understanding of the quantitative difference with [23] on the In concentration at which the single-band N_H changes sign. While there could be a small difference in concentration of Sn vacancies, that is unlikely to be the explanation, as the measured values of lattice parameter and superconducting transition temperature as a function of x [15,23] are rather consistent, which would not be the case for a significant difference in Sn vacancies [26].)

The apparent sharp jump in carrier concentration and sign with doping is surprising. If we look at the measured Hall coefficient at a temperature of 5 K, shown by the circles in Fig. 2(e), we see that it varies smoothly with doping. To understand what may be going on, we consider the behavior of the In dopants. An In atom has an outer $5s^25p^1$ configuration. When doped into SnTe, it will certainly give up its outer $5p$ electron to yield In^{+1}. Past work [17] has demonstrated that the In $5s$ level lies below the chemical potential of SnTe. For reference, the In-Te bond length in an In^{3+} compound such as In_2Te_3 is 2.67 Å [27], whereas the Sn-Te bond length in SnTe is 3.16 Å [15]; hence, it is plausible that the $5s$ electrons of an isolated In dopant will not hybridize with Te neighbors. Hybridization between In ions will only occur as the probability of In dopants being near one another becomes significant. Indeed, band structure calculations by Haldolaarachchige *et al.* [23] for $x = 0.12$ yield a narrow extra band, largely below the chemical potential. If the chemical potential shifts into this band, then the dominant carriers may become electronlike.
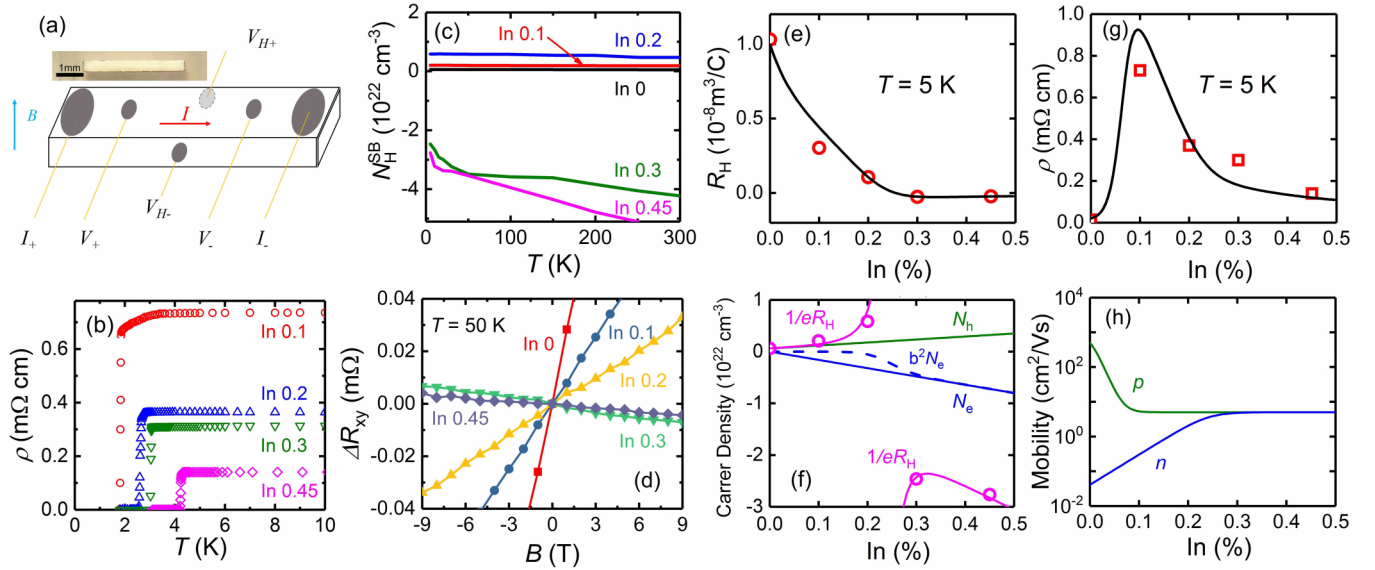
FIG. 2. Transport measurements on $Sn_{1-x}In_xTe$ samples. (a) Sketch of the contact locations on the sample. Inset shows a typical single crystal sample prepared for transport measurements (length $\sim$6 mm). (b) Resistivity vs temperature for various In concentrations; note that the superconducting transition increases with x. (c) Temperature dependent Hall carrier concentration N_H calculated using single band model $N_H = 1/eR_H$. A change of dominant carrier type occurs between $x = 0.2$ and 0.3. (d) Transverse resistance R_{xy} as a function of magnetic field B, at $T = 50$ K. (e) Hall coefficient at 5 K vs In doping (circles); line is a fit with the two-band model described in the text. (f) Plot of carrier concentrations N_h (green line) and N_e (blue line) assumed in the model calculation; dashed line represents the N_e multiplied by the squared ratio of mobilities, as discussed in the text. Circles indicate $1/eR_H$ data; magenta line is the model calculation. (g) Resistivity at 5 K (squares), compared with the model calculation (line). (Data point at $x = 0$ from [13].) (h) Hole and electron mobilities used in the model calculations.

We imagine a scenario as illustrated in Fig. 3; note that our synthesis differs in some details from previous work [17,23]. For $x = 0$, the chemical potential of SnTe lies in the valence band, due to a small density of Sn vacancies. For small but finite x, the In $5s$ electrons are localized near the In dopant sites, with the energy level lying below the initial chemical potential. Because of the $5s$ localization, the In ions act effectively as In^{+1}, causing the chemical potential to drop. This is consistent with previous transport results [13,20,28] that N_h is finite even at $x = 0$, grows with x up to at least $x \sim 0.1$, while ARPES studies [21,22] suggest that the hole pockets continue to grow slowly at larger x. At large enough x, the In $5s$ states form a narrow band and the chemical potential gets pinned in this

band. At this point, the In ions act as In^{3+} and electronlike carriers become important.

To approximately describe this behavior, we consider a two-band model that contains contributions from both holes and electrons [29]:

$$R_H = \frac{(N_h - N_e b^2)}{e(N_h + N_e b)^2},$$ (1)

where N_h (N_e) is the density of holes (electrons) and $b = \mu_e/\mu_h$, the ratio of mobilities of the electrons and holes. We take N_h to be small but finite at $x = 0$ and allow it to grow linearly with x. In contrast, we take N_e to be equal to the density of In ions, but make the mobility μ_e very small in the regime where the electrons are localized. The key to the crossover in dominant carrier type is the variation in the mobility ratio b which starts out small, but then grows rapidly towards one at larger x; the product $N_e b^2$ is indicated by the dashed line in Fig. 2(f). With these choices, we obtain the solid line in Fig. 2(e), which gives a good description of $R_H(x)$.

Of course, in modeling R_H [30] we have introduced more degrees of freedom than we have constraints. To test the model further, it is useful to consider the magnitude of ρ, which depends on both the carrier densities and the mobilities. The mobility can be quite large for SnTe at low temperature [31], but even 1% In doping raises the resistivity almost two orders of magnitude [13], implying a huge drop in mobility. From the reported resistivity for $x = 0$ [13] and our measurement of R_H, we estimate an initial hole mobility of $\sim$500 cm^2/(V s) (small compared to values in [31]); it then drops rapidly on the introduction of In, decreasing by two orders of magnitude by $x \sim 0.1$. We assume that the hole mobility then remains con-
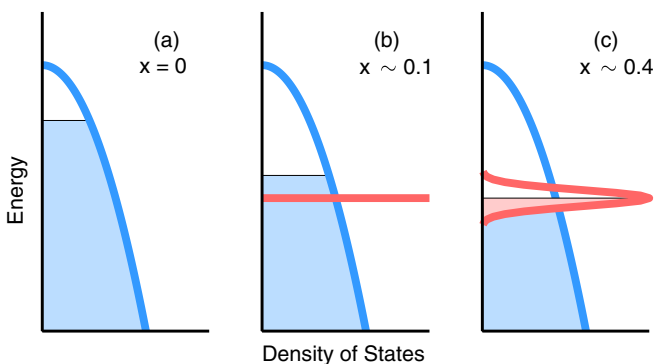
FIG. 3. Cartoon of the hole (blue) and electron (red) densities of states vs energy for $Sn_{1-x}In_xTe$, as discussed in the text: (a) $x = 0$; (b) $x \sim 0.1$; (c) $x \sim 0.4$.
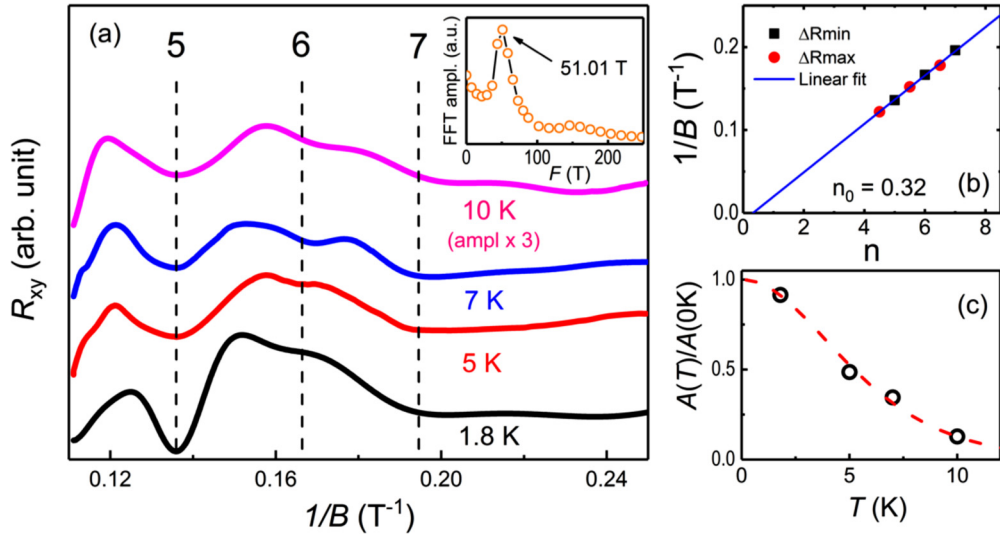
FIG. 4. (a) SdH oscillations in $Sn_{0.55}In_{0.45}Te$ transverse resistance measured at temperatures of 1.5 to 10 K plotted vs inverse magnetic field, after subtraction of conventional Hall response. The 10 K data are multiplied by 3, and curves have been offset vertically. The assigned Landau level indices are indicated by the numbered vertical dashed lines. Inset shows fast Fourier transform (FFT) spectrum of the 5 K data. (b) Plot of inverse field for oscillation extrema vs Landau level index; linear fit yields an intercept of 0.32 ± 0.07. (c) The temperature dependence of the oscillation amplitude at $n = 5$ fitted by Lifshitz-Kosevich theory (dashed line), yielding a cyclotron mass m_{cycl} of $0.185m_e$.

stant at 5 cm^2/(V s). Meanwhile, the electron mobility starts out at a negligible level (where the electrons are localized) and steadily rises, becoming comparable to the hole mobility at $x \sim 0.25$. Using the model mobilities plotted in Fig. 2(h) together with the carrier densities shown in Fig. 2(f), we obtain for ρ the solid line plotted in Fig. 2(g), which certainly captures the trend of the experimental data points.

B. Quantum oscillations

Measurements of the field dependence of R_H for the $x = 0.45$ sample with the field along (001) revealed prominent SdH oscillations. Figure 4(a) shows the oscillations in the transverse resistance at 10 K and below, after subtracting backgrounds, revealing periodic behavior as a function of inverse field. The positions of the peaks and valleys appear to be independent of temperature, though the magnitude is not. Analysis of these features can provide parameters related to the relevant portions of the Fermi surface. The inset in Fig. 4(a) shows the amplitude of the Fourier transform of the 5 K SdH spectrum yielding the frequency $f_{SdH} = 51$ T. The cross section of the Fermi surface A_F is related to the SdH oscillation frequency via the Onsager relation [32]: $f_{SdH} = (h/4\pi^2 e)A_F$, where $A_F = \pi k_F^2$, with k_F being the Fermi wave vector. The resulting k_F is 0.04 Å^{-1}.

The Landau level index has been assigned as done in previous reports [32–35], and the positions of the peaks and valleys measured in inverse field are plotted as a function of Landau level index n in Fig. 4(b). The linear fit leads to a nonzero intercept of 0.32 ± 0.07, a value comparable to 0.5 which is expected for massless Dirac fermions, more commonly for surface states in TIs [32–37].

Given the substantial carrier density in our sample, we expect that the quantum oscillations must come from bulk states. Of course we have both hole- and electronlike carriers, so which of these contributes the oscillations? ARPES studies

of SIT have observed the hole pockets near the L points, and have distinguished bulk and surface states by their dispersion with momentum perpendicular to the sample surface [21,22]. For a sample with $x \approx 0.4$, both the bulk and surface states show a Dirac-like dispersion near the hole pockets, while no electronlike features have been identified [22]. Hence, it seems most plausible to associate the oscillations with bulk holelike pockets.

Figure 4(c) shows the temperature dependence of the SdH amplitude $A(T)$ at $n = 5$, fitted with the Lifshitz-Kosevich theory [38]: $A(T) = \lambda/\sinh\lambda$, where $\lambda = (\pi k_B T/ehB)m_{cycl}$. The cyclotron mass m_{cycl} is found to be $0.185m_e$ at a field of 6.5 T, where m_e is the free electron mass. Assuming a Dirac-like dispersion, the Fermi velocity v_F can be calculated by $v_F m_{cycl} = \hbar k_F$ [32,35], yielding 2.5×10^5 m/s.

We can compare our results with those obtained by ARPES for the bulk L-point pockets of a (111) SIT film with $x \approx 0.4$ [22]. The latter study found a linear dispersion characterized by $k_F = 0.095$ Å^{-1} and a Fermi velocity of 6.0×10^5 m/s, which puts the Fermi level 0.38 eV below an extrapolated Dirac point. This compares with our $k_F = 0.04$ Å^{-1} and $v_F = 2.5 \times 10^5$ m/s, which would put the Fermi level at 0.07 eV. The main point here is that the values are of comparable magnitude.

C. Magnetoresistance

Observations of WAL [39] in low-temperature magnetoresistance measurements on pristine SnTe have been used to identify the presence of topologically protected surface states [9,10]. Recent theoretical work has demonstrated that one can also observe WAL from bulk Dirac-like states with strong spin-orbit coupling [24]. Now, WAL from surface states should be sensitive to the orientation of the magnetic field with respect to the surface [40]. Below we demonstrate WAL that is insensitive to field direction, consistent with bulk Dirac-like
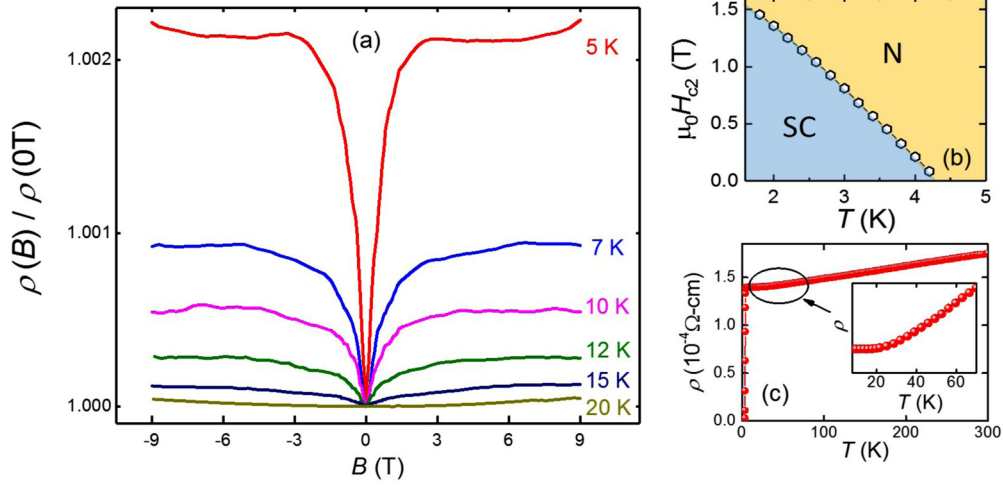
FIG. 5. Normalized longitudinal resistivity for the $Sn_{0.55}In_{0.45}Te$ single crystal. (a) Magnetoresistance curves exhibit a sharp cusp at $B = 0$ with an amplitude that diminishes with increasing temperature. (b) Phase diagram of $Sn_{0.55}In_{0.45}Te$ showing the upper critical field vs temperature [15]. (c) Zero-field resistivity over an extended temperature range; inset shows that there is a plateau below 20 K, where the MR develops.

states, which, based on the analysis of the SdH oscillations, are likely associated with the holelike pockets near the L points.

Figure 5(a) shows the normalized longitudinal magnetoresistance (MR) $\rho(B)/\rho(0\,T)$ obtained with the magnetic field applied perpendicular to the current for the $Sn_{0.55}In_{0.45}Te$ sample. The magnitude of the MR increases rapidly on cooling below 20 K. Note that we are limited in temperature range by the superconducting transition; for reference, the superconducting phase diagram is shown in Fig. 5(b). The rapid rise and saturation looks very much like the WAL that has been observed in association with topologically protected surface states in TIs such as Bi_2Te_3 [40]. Similar behavior was observed for our $x = 0.3$ sample, but with a reduced magnitude. Figure 5(c) shows the temperature dependence of the zero-field resistivity, indicating a saturation below 20 K, corresponding to the region where the sharp MR appears.

As noted above, MR from surface states should be sensitive to the orientation of the magnetic field. To test this, angle-dependent MR was measured at 5 K. As shown in the inset of Fig. 6, θ and ϕ denote the angles between the magnetic field and z axis within x-z and y-z planes, respectively, where the electrical current is always applied along the x direction. We observe that the low-field MR is essentially independent of angle. This isotropic response indicates bulk behavior.

For WAL from bulk states [24], the contribution to the conductance has the same form as that for the two-dimensional case [39]:

$$\Delta G = \alpha \frac{e^2}{\pi h}\left[\ln\left(\frac{B_\phi}{B}\right) - \psi\left(\frac{B_\phi}{B} + \frac{1}{2}\right)\right], \qquad (2)$$

where ψ is the digamma function and $B_\phi = \phi_0/(8\pi l_\phi^2)$, with $\phi_0 = h/e$ and l_ϕ being the phase coherence length. The

FIG. 6. Angle-dependent magnetoresistance measurements for $Sn_{0.55}In_{0.45}Te$ at 5 K. The cusp appears to be independent of orientation of applied magnetic field. Inset defines the orientation angles of the applied magnetic field relative to the sample surface and direction of applied current.
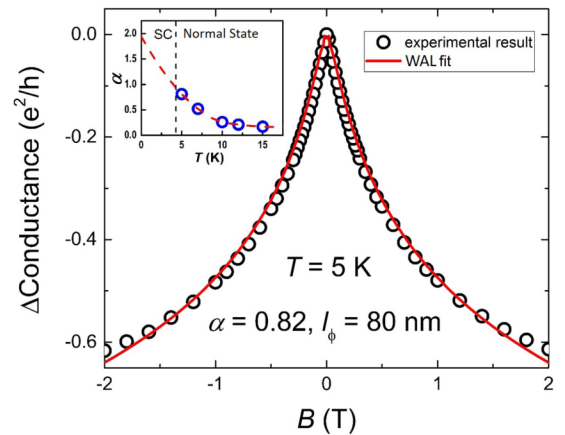
FIG. 7. Conductance change with magnetic field for $Sn_{0.55}In_{0.45}Te$ at 5 K. Circles denote experimental data; line is a fit to the WAL formula (see text) with $\alpha = 0.82$ and $l_\phi = 80$ nm. Inset shows the temperature dependence of α; dashed line shows an extrapolation to low temperature.

parameter α is a constant that equals 1 for the case of Dirac-like dispersion in a single pocket at the Brillouin zone center [24] (which is slightly different from our case of pockets at the L points).

In Fig. 7 we plot the experimental ΔG obtained at 5 K. The line through the data points is a fit with Eq. (2), which yields the parameters $\alpha = 0.82$ and $l_\phi = 80$ nm. The value of α is temperature dependent, as shown in the inset; it extrapolates towards ~ 2 at low temperature.

V. CONCLUSION

We have used transport measurements to study the normal state of $Sn_{1-x}In_xTe$ crystals across much of the composition range for which superconductivity occurs. We have confirmed that the dominant carrier type changes from holelike to electronlike near $x \sim 0.25$. The observations of quantum oscillations and a bulk WAL response in the magnetoresistance at $x = 0.45$ provide evidence for the holelike states that have been detected by ARPES about the L points of the bulk Brillouin zone. Hence, holelike and electronlike carriers coexist and all contribute to the transport.

In modeling the doping dependence of the Hall effect, we considered a picture in which the In $5s$ states sit somewhat below the chemical potential of SnTe. At low concentration, these states behave as if they are localized, so that the chemical potential moves lower in the valence band. With increasing concentration, the In $5s$ levels begin to hybridize with one another, and these electronlike states gain some mobility. In the future it would be interesting to see this picture tested with spectroscopic measurements, with a particular focus on characterizing the electronlike states.

This mixture of carriers is of interest with respect to the nature of the superconductivity. The superconducting transition temperature rises continuously with In concentration across the crossover in dominant carrier type [13–15,23], so presumably both kinds of carriers can contribute to the condensate. Is the presence of multiple bands relevant to the pairing mechanism? Or, given the modest carrier mobility, are the interactions with the lattice of a more local character? It was noted quite some time ago that the nonionic bonding character of IV-VI compounds with the rock salt structure leads to a significant electron-phonon interaction [41,42]. Indeed, an enhanced damping has been observed for low-energy transverse acoustic phonons in $Sn_{0.8}In_{0.2}Te$ [43]. What role does the strong electronic polarizability play in the localization/delocalization of the In $5s$ states, and how does this relate to evidence for strong-coupling superconductivity [23]? Of course, there is also the question of whether there is any topological character to the superconducting state [16,44]. There is clearly more to explore in this system.

ACKNOWLEDGMENTS

[1] J. E. Moore, The birth of topological insulators, Nature (London) **464**, 194 (2010).

[2] M. Z. Hasan and C. L. Kane, Colloquium: Topological insulators, Rev. Mod. Phys. **82**, 3045 (2010).

[3] X.-L. Qi and S.-C. Zhang, Topological insulators and superconductors, Rev. Mod. Phys. **83**, 1057 (2011).

[4] L. Fu, Topological Crystalline Insulators, Phys. Rev. Lett. **106**, 106802 (2011).

[5] T. H. Hsieh, H. Lin, J. Liu, W. Duan, A. Bansil, and L. Fu, Topological crystalline insulators in the SnTe material class, Nat. Commun. **3**, 982 (2012).

[6] S.-Y. Xu, C. Liu, N. Alidoust, M. Neupane, D. Qian, I. Belopolski, J. D. Denlinger, Y. J. Wang, H. Lin, L. A. Wray, G. Landolt, B. Slomski, J. H. Dil, A. Marcinkova, E. Morosan, Q. Gibson, R. Sankar, F. C. Chou, R. J. Cava, A. Bansil, and M. Z. Hasan, Observation of a topological crystalline insulator phase and topological phase transition in $Pb_{1x}Sn_xTe$, Nat. Commun. **3**, 1192 (2012).

[7] P. B. Littlewood, B. Mihaila, R. K. Schulze, D. J. Safarik, J. E. Gubernatis, A. Bostwick, E. Rotenberg, C. P. Opeil, T. Durakiewicz, J. L. Smith, and J. C. Lashley, Band Structure of SnTe Studied by Photoemission Spectroscopy, Phys. Rev. Lett. **105**, 086404 (2010).

[8] Y. Tanaka, Z. Ren, T. Sato, K. Nakayama, S. Souma, T. Takahashi, K. Segawa, and Y. Ando, Experimental realization of a topological crystalline insulator in SnTe, Nat. Phys. **8**, 800 (2012).

[9] B. A. Assaf, F. Katmis, P. Wei, B. Satpati, Z. Zhang, S. P. Bennett, V. G. Harris, J. S. Moodera, and D. Heiman, Quantum coherent transport in SnTe topological crystalline insulator thin films, Appl. Phys. Lett. **105**, 102108 (2014).

[10] R. Akiyama, K. Fujisawa, R. Sakurai, and S. Kuroda, Weak antilocalization in (111) thin films of a topological crystalline insulator SnTe, J. Phys.: Conf. Ser. **568**, 052001 (2014).

[11] L. Fu and C. L. Kane, Superconducting Proximity Effect and Majorana Fermions at the Surface of a Topological Insulator, Phys. Rev. Lett. **100**, 096407 (2008).

[12] X.-L. Qi, T. L. Hughes, S. Raghu, and S.-C. Zhang, Time-Reversal-Invariant Topological Superconductors and Superfluids in Two and Three Dimensions, Phys. Rev. Lett. **102**, 187001 (2009).

[13] A. S. Erickson, J.-H. Chu, M. F. Toney, T. H. Geballe, and I. R. Fisher, Enhanced superconducting pairing interaction in indium-doped tin telluride, Phys. Rev. B **79**, 024520 (2009).

[14] G. Balakrishnan, L. Bawden, S. Cavendish, and M. R. Lees, Superconducting properties of the In-substituted topological crystalline insulator SnTe, Phys. Rev. B **87**, 140507 (2013).

[15] R. D. Zhong, J. A. Schneeloch, X. Y. Shi, Z. J. Xu, C. Zhang, J. M. Tranquada, Q. Li, and G. D. Gu, Optimizing the superconducting transition temperature and upper critical field of $Sn_{1-x}In_xTe$, Phys. Rev. B **88**, 020505 (2013).

[16] S. Sasaki, Z. Ren, A. A. Taskin, K. Segawa, L. Fu, and Y. Ando, Odd-Parity Pairing and Topological Superconductivity in

a Strongly Spin-Orbit Coupled Semiconductor, Phys. Rev. Lett. **109**, 217004 (2012).

[17] V. I. Kaĭdanov and Yu. I. Ravich, Deep and resonance states in A IV B VI semiconductors, Sov. Phys. Usp. **28**, 31 (1985).

[18] Y. Matsushita, P. A. Wianecki, A. T. Sommer, T. H. Geballe, and I. R. Fisher, Type II superconducting parameters of Tl-doped PbTe determined from heat capacity and electronic transport measurements, Phys. Rev. B **74**, 134512 (2006).

[19] P. Giraldo-Gallo, P. Walmsley, B. Sangiorgio, S. C. Riggs, R. D. McDonald, L. Buchauer, B. Fauque, C. Liu, N. A. Spaldin, A. Kaminski, K. Behnia, and I. R. Fisher, Evidence of incoherent carriers associated with resonant impurity levels and their influence on superconductivity in the anomalous superconductor $Pb_{1-x}Tl_xTe$, arXiv:1711.05723 .

[20] J. Shen, Y. Xie, and J. J. Cha, Revealing surface states in in-doped SnTe nanoplates with low bulk mobility, Nano Lett. **15**, 3827 (2015).

[21] T. Sato, Y. Tanaka, K. Nakayama, S. Souma, T. Takahashi, S. Sasaki, Z. Ren, A. A. Taskin, K. Segawa, and Y. Ando, Fermiology of the Strongly Spin-Orbit Coupled Superconductor $Sn_{1-x}In_xTe$: Implications for Topological Superconductivity, Phys. Rev. Lett. **110**, 206804 (2013).

[22] C. M. Polley, V. Jovic, T.-Y. Su, M. Saghir, D. Newby, B. J. Kowalski, R. Jakiela, A. Barcz, M. Guziewicz, T. Balasubramanian, G. Balakrishnan, J. Laverock, and K. E. Smith, Observation of surface states on heavily indium-doped SnTe(111), a superconducting topological crystalline insulator, Phys. Rev. B **93**, 075132 (2016).

[23] N. Haldolaarachchige, Q. Gibson, W. Xie, M. B. Nielsen, S. Kushwaha, and R. J. Cava, Anomalous composition dependence of the superconductivity in In-doped SnTe, Phys. Rev. B **93**, 024520 (2016).

[24] I. Garate and L. Glazman, Weak localization and antilocalization in topological insulator thin films with coherent bulk-surface coupling, Phys. Rev. B **86**, 035422 (2012).

[25] P. Blaha, K. Schwarz, P. Sorantin, and S. B. Trickey, Full-potential, linearized augmented plane wave programs for crystalline systems, Comput. Phys. Commun. **59**, 399 (1990).

[26] G. S. Bushmarina, I. A. Drabkin, V. V. Kompaniets, R. V. Parfen'ev, D. V. Shamshur, and M. A. Shakov, Superconducting transition in indium-alloyed SnTe, Sov. Phys. Solid State **28**, 612 (1986).

[27] J. C. Woolley, B. R. Pamplin, and P. J. Holmes, The ordered crystal structure of In_2Te_3, J. Less Common Met. **1**, 362 (1959).

[28] G. S. Bushmarina, B. F. Gruzinov, I. A. Drabkin, E. Ya. Lev, and V. M. Yuneev, Characteristics of the effects of In as a dopant in SnTe, Sov. Phys. Semicond. **18**, 1374 (1984).

[29] N. W. Ashcroft and N. D. Mermin, *Solid State Physics* (Holt, Rinehart, and Winston, New York, 1976), p. 240.

[30] We note that there are field-dependent corrections to Eq. (1) which predict curvature in R_{xy} that are not seen in the data of Fig. 2(d). We simply take this as a shortcoming of our crude model.

[31] R. S. Allgaier and B. Houston, Weak-field magnetoresistance and the valence-band structure of SnTe, Phys. Rev. B **5**, 2186 (1972).

[32] L. Bao, L. He, N. Meyer, X. Kou, P. Zhang, Z.-g. Chen, A. V. Fedorov, J. Zou, T. M. Riedemann, T. A. Lograsso, K. L. Wang, G. Tuttle, and F. Xiu, Weak Anti-localization and quantum oscillations of surface states in topological insulator Bi_2Se_2Te, Sci. Rep. **2**, 726 (2012).

[33] D.-X. Qu, Y. S. Hor, J. Xiong, R. J. Cava, and N. P. Ong, Quantum oscillations and Hall anomaly of surface states in the topological insulator Bi_2Te_3, Science **329**, 821 (2010).

[34] J. Xiong, A. C. Petersen, D. Qu, Y. S. Hor, R. J. Cava, and N. P. Ong, Quantum oscillations in a topological insulator Bi_2Te_2Se with large bulk resistivity (6 Ω cm), Physica E **44**, 917 (2012).

[35] Z. Ren, A. A. Taskin, S. Sasaki, K. Segawa, and Y. Ando, Large bulk resistivity and surface quantum oscillations in the topological insulator Bi_2Te_2Se, Phys. Rev. B **82**, 241306 (2010).

[36] J. G. Analytis, R. D. McDonald, S. C. Riggs, J.-H. Chu, G. S. Boebinger, and I. R. Fisher, Two-dimensional surface state in the quantum limit of a topological insulator, Nat. Phys. **6**, 960 (2010).

[37] T.-C. Hsiung, D.-Y. Chen, L. Zhao, Y.-H. Lin, C.-Y. Mou, T.-K. Lee, M.-K. Wu, and Y.-Y. Chen, Enhanced surface mobility and quantum oscillations in topological insulator $Bi_{1.5}Sb_{0.5}Te_{1.7}Se_{1.3}$ nanoflakes, Appl. Phys. Lett. **103**, 163111 (2013).

[38] D. Shoenberg, *Magnetic Oscillations in Metals* (Cambridge University Press, Cambridge, 1984).

[39] S. Hikami, A. I. Larkin, and Y. Nagaoka, Spin-orbit interaction and magnetoresistance in the two dimensional random system, Prog. Theor. Phys. **63**, 707 (1980).

[40] H.-T. He, G. Wang, T. Zhang, I.-K. Sou, G. K. L Wong, J.-N. Wang, H.-Z. Lu, S.-Q. Shen, and F.-C. Zhang, Impurity Effect on Weak Antilocalization in the Topological Insulator Bi_2Te_3, Phys. Rev. Lett. **106**, 166805 (2011).

[41] G. Lucovsky and R. M. White, Effects of resonance bonding on the properties of crystalline and amorphous semiconductors, Phys. Rev. B **8**, 660 (1973).

[42] P. B. Littlewood and V. Heine, The infrared effective charge in IV-VI compounds. I. A simple one-dimensional model, J. Phys. C: Solid State Phys. **12**, 4431 (1979).

[43] Z. Xu, J. A. Schneeloch, R. D. Zhong, J. A. Rodriguez-Rivera, L. W. Harriger, R. J. Birgeneau, G. D. Gu, J. M. Tranquada, and G. Xu, Low-energy phonons and superconductivity in $Sn_{0.8}In_{0.2}Te$, Phys. Rev. B **91**, 054522 (2015).

[44] M. P. Smylie, H. Claus, W.-K. Kwok, E. R. Louden, M. R. Eskildsen, A. S. Sefat, R. D. Zhong, J. Schneeloch, G. D. Gu, E. Bokari, P. M. Niraula, A. Kayani, C. D. Dewhurst, A. Snezhko, and U. Welp, Superconductivity, pairing symmetry, and disorder in the doped topological insulator $Sn_{1-x}In_xTe$ for $x \geqslant 0.10$, Phys. Rev. B **97**, 024511 (2018).